Distinct Colorectal Cancer–Associated APC Mutations Dictate Response to Tankyrase Inhibition

Emma M. Schatoff[1,2,3], Sukanya Goswami[1], Maria Paz Zafra[1], Miguel Foronda[1], Michael Shusterman[1], Benjamin I. Leach[1], Alyna Katti[1,3], Bianca J. Diaz[1,3], and Lukas E. Dow[1,3,4]

ABSTRACT

The majority of colorectal cancers show hyperactivated WNT signaling due to inactivating mutations in the adenomatous polyposis coli (APC) tumor suppressor. Genetically restoring APC suppresses WNT and induces rapid and sustained tumor regression, implying that reengaging this endogenous tumor-suppressive mechanism may be an effective therapeutic strategy. Here, using new animal models, human cell lines, and *ex vivo* organoid cultures, we show that tankyrase (TNKS) inhibition can control WNT hyperactivation and provide long-term tumor control *in vivo*, but that effective responses are critically dependent on how APC is disrupted. Mutant APC proteins truncated within the mutation cluster region physically engage the destruction complex and suppress the WNT transcriptional program, while APC variants with early truncations (e.g., Apc^{Min}) show limited interaction with AXIN1 and β-catenin, and do not respond to TNKS blockade. Together, this work shows that TNKS inhibition, like APC restoration, can reestablish endogenous control of WNT/β-catenin signaling, but that APC genotype is a crucial determinant of this response.

SIGNIFICANCE: This study reveals how subtle changes to the mutations in a critical colorectal tumor suppressor, APC, influence the cellular response to a targeted therapy. It underscores how investigating the specific genetic alterations that occur in human cancer can identify important biological mechanisms of drug response and resistance.

INTRODUCTION

Hyperactivation of the WNT signaling pathway is a hallmark of colorectal cancer, in most cases (~80%) due to inactivating mutations in the adenomatous polyposis coli (APC) tumor suppressor (1, 2). APC is a scaffold protein that coordinates assembly of the destruction complex (DC), which is made up of core proteins APC, AXIN1, GSK3β, and CK1α. The DC regulates WNT signaling via sequential phosphorylation of the WNT master regulator β-catenin, marking it for degradation by the proteasome (3). Previously, using genetically

[1]Sandra and Edward Meyer Cancer Center, Department of Medicine, Weill Cornell Medicine, New York, New York. [2]Weill Cornell/Rockefeller/Sloan Kettering Tri-I MD-PhD program, New York, New York. [3]Weill Cornell Graduate School of Medical Sciences, Weill Cornell Medicine, New York, New York. [4]Department of Biochemistry, Weill Cornell Medicine, New York, New York.

Note: Supplementary data for this article are available at Cancer Discovery Online (http://cancerdiscovery.aacrjournals.org/).

Corresponding Author: Lukas E. Dow, Weill Cornell Medicine, Belfer Research Building, 413 E 69th Street, BB1318, New York, NY 10044. Phone: 646-962-6313; E-mail: lud2005@med.cornell.edu

Cancer Discov 2019;9:1358–71

doi: 10.1158/2159-8290.CD-19-0289

engineered and transplantation-based mouse models, we showed that restoration of endogenous APC expression drives WNT suppression and rapid regression of colorectal cancers in both the colon and liver (4, 5). This work provides *in vivo* evidence that reengaging endogenous regulation of WNT signaling is a potent tumor-suppressive strategy.

Pharmacologically, it is possible to reengage DC activity via tankyrase inhibition (6). Tankyrase 1 and 2 (TNKS1/2) are functionally redundant members of the PARP family. Unlike other PARP proteins, they play no role in DNA repair, but rather potentiate WNT signaling by PARylating AXIN1/2, targeting it for degradation, and decreasing the stability and activity of the DC (7–9). Numerous small molecules that enable selective TNKS1/2 blockade and WNT-pathway suppression in colorectal cancer cell lines (10–12) and normal mouse intestine (13, 14) have been described, yet evidence for suppression of WNT-driven tumor growth *in vivo* is conflicting (15–17). Thus, it is unclear whether, and in what context, reengaging the tumor-suppressive DC is an effective approach to control hyperactive WNT/β-catenin signaling. Given the well-defined and consistent tumor response seen following APC restoration in sh*Apc* mice, we sought to exploit genetically defined *in vivo* and organoid models to determine how TNKS inhibition influences tumor cell behavior after APC disruption.

RESULTS

We previously showed that the acute response to APC restoration in intestinal and colonic tumors is cell-cycle arrest and differentiation (4, 5). To determine whether TNKS1/2 inhibition could elicit a similar response *in vivo*, we established a cohort of tumor-bearing *CAGs-LSL-rtTA3/TRE-GFP-shApc/Lgr5-CreER* (hereafter *TG-shApc*) mice by treatment with 4-hydroxytamoxifen (4OHT; 25 mg/kg, single intraperitoneal injection) and doxycycline (200 mg/kg in the chow, *ad libitum*; Fig. 1A; Supplementary Fig. S1A). Eight to 12 weeks following tumor initiation, mice were randomized into two treatment arms: TNKS1/2 inhibitor G007-LK (30 mg/kg, once daily; ref. 16) or vehicle control, for 1 week. Vehicle-treated mice showed highly proliferative lesions with elevated expression of the stem-cell marker LGR5, and limited and sporadic evidence of differentiation markers Keratin 20 (KRT20) and intestinal alkaline phosphatase (ALPi; Fig. 1B). In contrast, G007-LK–treated and APC-restored tumors had reduced BrdU incorporation, loss of LGR5 expression, and induction of both KRT20 and ALPi (Fig. 1B–C). Thus, pharmacologic TNKS1/2 inhibition phenocopies the acute, tumor cell–intrinsic response to genetic restoration of APC.

We next sought to confirm our findings in an independent APC-driven colorectal cancer model. Apc^{Min} mice carry a heterozygous nonsense mutation at codon 850 of *Apc* and develop intestinal tumors following spontaneous loss of the wild-type allele (18). We treated tumor-bearing 15- to 20-week-old Apc^{Min} mice for 1 week with G007-LK (30 mg/kg, once daily) and measured tumor response on histologic cross-sections, as described above. Surprisingly, and in contrast to what we observed in the *TG-shApc* model, Apc^{Min} tumors were completely insensitive to G007-LK treatment. In fact, whereas adjacent normal intestine showed elevated AXIN1 and decreased LGR5 staining, confirming drug exposure (Supplementary Fig. S1B and S1C), G007-LK–treated tumors maintained proliferation and LGR5 expression, and showed minimal KRT20 staining or ALPi activity (Fig. 1C and D).

The difference in tumor response between these two APC-driven models was striking, and was in contrast to a recent report by Tanaka and colleagues, which suggested that early truncating mutations in APC sensitize cell lines to TNKS inhibition (19). To ensure this conflicting effect was not due to differences in *in vivo* tumor growth kinetics or timing of treatment, we generated sh*Apc* and Apc^{Min} intestinal organoids and treated them *ex vivo* for 3 days with G007-LK (1 μmol/L). In support of our *in vivo* results, G007-LK–treated sh*Apc* organoids underwent rapid cell-cycle arrest, whereas Apc^{Min} organoids maintained a proliferative phenotype (Fig. 1E). RNA expression measured by quantitative RT-PCR (qPCR) further confirmed that TNKS1/2 inhibition induced *Krt20* and reduced *Lgr5* expression in sh*Apc* organoids, but had no effect in Apc^{Min} cultures (Fig. 1F). Together, these data support the notion that TNKS inhibition can effectively promote tumor-cell arrest in some contexts.

Although BrdU incorporation was significantly decreased in G007-LK–treated sh*Apc* tumors, the response was less uniform than that following genetic APC restoration (Fig. 1B), raising the possibility that variable drug dose or delivery may have affected tumor response in some cases. Indeed, current TNKS inhibitors show limited oral bioavailability and require daily or twice-daily intraperitoneal or intratumoral delivery to achieve effective TNKS blockade (16, 20). In addition, in our hands, daily intraperitoneal dosing also produced inflammatory adhesions on the liver, spleen, and peritoneum, precluding increased or prolonged treatment (Supplementary Fig. S1D). To achieve potent, constitutive TNKS blockade without the confounding issue of drug delivery, we produced two new transgenic strains (carrying independent tandem shRNAs) that enable doxycycline-inducible silencing of TNKS1/2. To do this, we first screened a series of TNKS and TNKS2 miRE-based shRNAs using a fluorescent sensor construct and identified the two most potent targeting each gene (Supplementary Fig. S2A–S2C). Importantly, both tandem sh*Tnks1/2* constructs induced AXIN1 stabilization comparable with treatment with a small-molecule TNKS inhibitor *in vitro* (Supplementary Fig. S2D) and *in vivo* (Supplementary Fig. S2E).

To assess the capacity of TNKS1/2 blockade to provide long-term tumor control, we crossed each *TG-shTnks1/2* strain to *TG-shApc* mice and treated 6- to 8-week-old mice with 4OHT and doxycycline (Fig. 2A). In sh*Apc* mice, numerous GFP^+ colon lesions were detectable as early as 4 weeks (Fig. 2B), and by 10 to 12 weeks (endpoint), tumors made up more than a quarter (28%) of the gut (Fig. 2C and D). In contrast, sh*Apc*/sh*Tnks* mice showed only individual GFP^+ crypts, similar to those seen in sh*Renilla* (sh*Ren*) control mice (Fig. 2B and C; Supplementary Fig. S3A). No adenomas were observed in the colon of sh*Apc*/sh*Tnks* mice up to 150 days (endpoint), at which time most sh*Apc* mice had become moribund (median survival 111 days; Fig. 2E). Similarly, the small intestine of sh*Apc*/sh*Tnks* animals resembled wild-type (WT) tissue, with only a few animals displaying small hyperproliferative lesions that made up 0.1% to 0.5% of the total intestinal area (Fig. 2D). Tumor suppression was not due to an off-target effect of the *Tnks* shRNAs, as we observed an identical effect using the

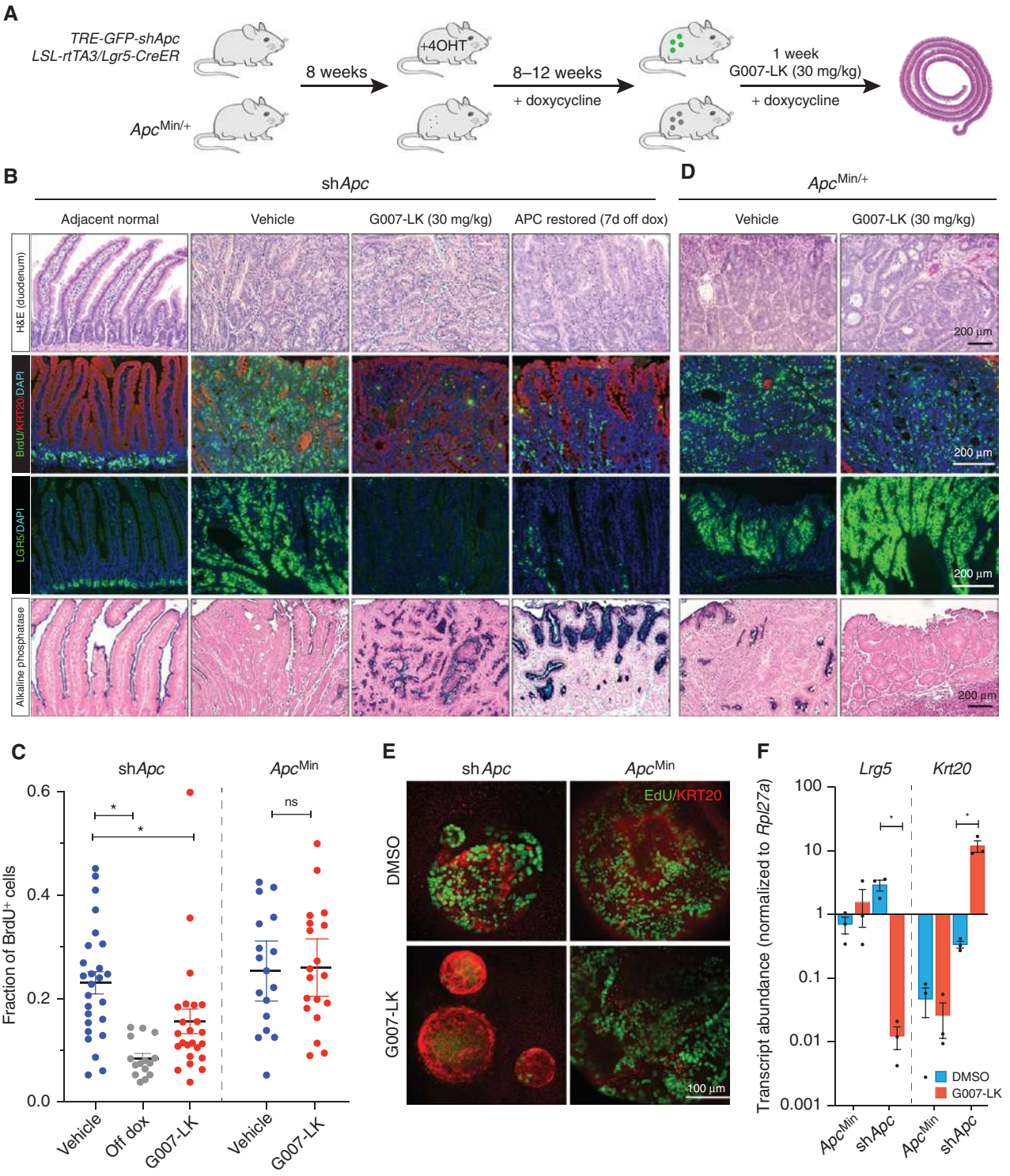

Figure 1. Tankyrase inhibition drives differentiation in APC-silenced intestinal tumors. **A,** Schematic depiction of the animal models and treatments to produce adenomas *in vivo*. For consistency, Apc^{Min} mice were administered doxycycline (dox) at 8 weeks (when tumors are first detectable), and continued for 8–12 weeks. sh*Apc* and Apc^{Min} mice were treated with G007-LK (30 mg/kg) or vehicle for 1 week, then sacrificed to assess tumor burden. **B,** IHC, immunofluorescence, and *in situ* hybridization (ISH; LGR5) stains of representative small intestinal adenomas from sh*Apc* mice as indicated. Adjacent normal crypt-villus architecture and sh*Apc* off doxycycline (1 week) are shown for reference. **C,** Quantitation of the fraction of BrdU-positive cells in individual tumors ($n = 3$–6 tumors/mouse; $n = 3$–6 mice/treatment). Bars show the mean and 95% CI. **D,** IHC, immunofluorescence, and ISH (LGR5) stains of representative small intestinal adenomas from Apc^{Min} mice as indicated. **E,** Immunofluorescence images of sh*Apc* and Apc^{Min} organoids cultured in DMSO or G007-LK (1 μmol/L) for 3 days. Organoids were pulsed with EdU for 4 hours to label proliferative cells. **F,** Quantitative RT-PCR analysis of gene expression of stem-cell (*Lgr5*) and differentiation (*Krt20*) markers in sh*Apc* and Apc^{Min} organoids cultured in DMSO or G007-LK (1 μmol/L) for 3 days ($n = 3$, error bars = s.e.m, *, $P < 0.05$, unpaired *t* test with Welch correction).

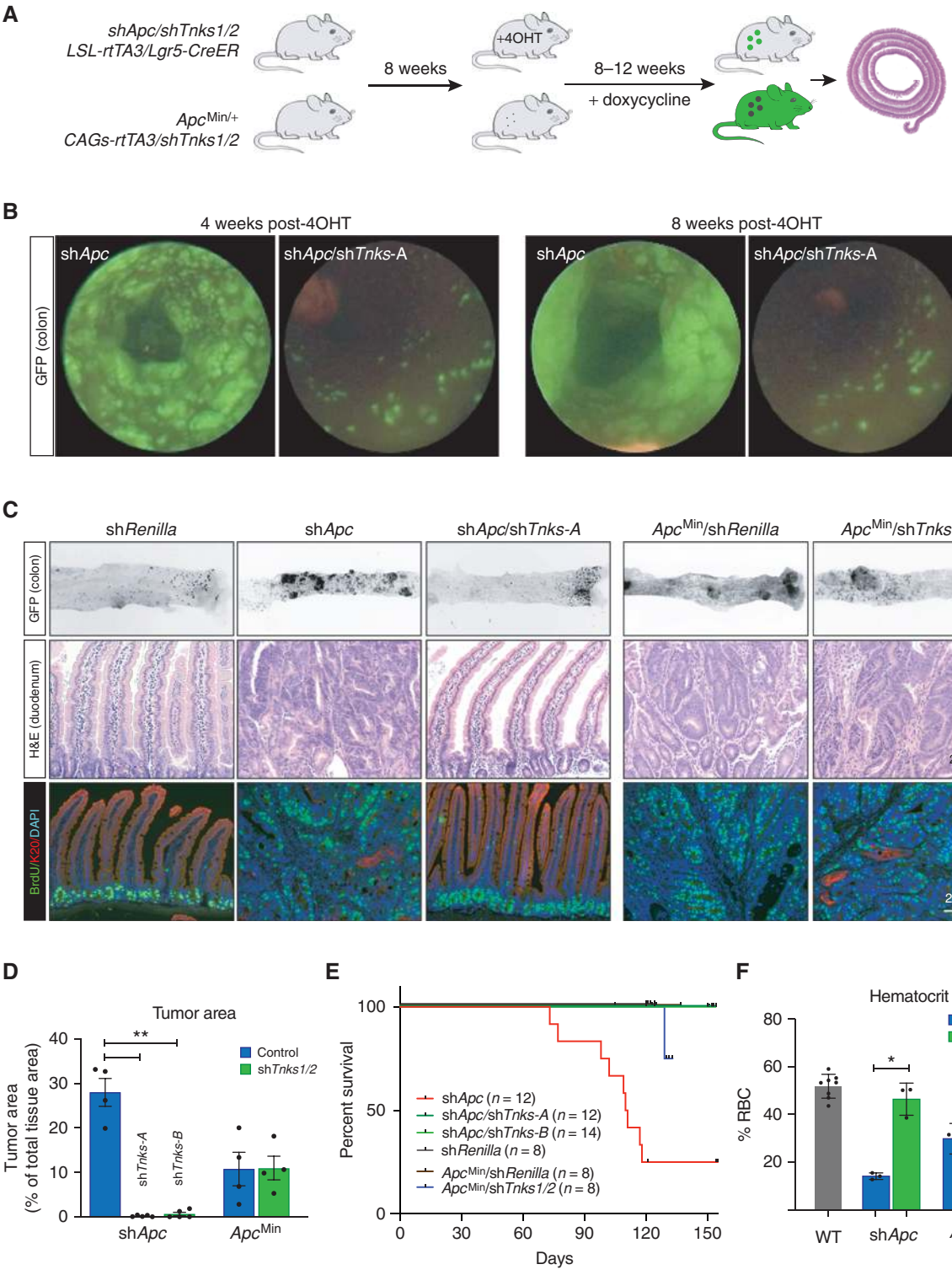

Figure 2. Sustained TNKS1/2 knockdown is sufficient to block sh*Apc*-mediated tumorigenesis. **A,** Schematic of the experimental strategy to achieve TNKS1/2 knockdown in sh*Apc* and Apc^{Min} adenomas. **B,** Colonic endoscopy images taken 4 and 8 weeks post 4OHT/doxycycline treatment in sh*Apc* or sh*Apc*/sh*Tnks1/2* mice show a dramatic difference in adenoma formation. **C,** Epifluorescence images of whole-mount colon from sh*Ren*, sh*Apc*, sh*Apc*/sh*Tnks1/2*, Apc^{Min}/sh*Ren*, and Apc^{Min}/sh*Tnks1/2* mice sacrificed at the experimental endpoint. Black signal represents GFP fluorescence. Immunohistochemical [hematoxylin and eosin (H&E)] and immunofluorescence (BrdU/KRT20) stains of representative small-intestinal adenomas from mice sacrificed at experimental endpoint. **D,** Quantitation of tumor burden from H&E-stained sections of each genotype, as indicated. Tumor area was calculated as a percentage of total tissue in representative cross-sections of the small intestine and colon ($n = 4$–5, error bars = SEM, **, $P < 0.005$, unpaired *t* test with Welch correction). **E,** Kaplan–Meier plot showing survival of each genotype, as indicated. Log-rank statistical tests are available in Supplementary Table S5. **F,** Hematocrit from peripheral blood of each genotype at experimental endpoint ($n = 3$–8, error bars = SEM, *, $P < 0.05$, unpaired *t* test with Welch correction). RBC, red blood cells.

second *TG-shTnks1/2* strain (Supplementary Fig. S3A–S3C). Consistent with the dramatically reduced tumor burden, sh*Apc*/sh*Tnks* mice showed no signs of the anemia (reduced hematocrit) that is commonly seen in sh*Apc* mice with substantial intestinal tumor load (Fig. 2F).

Mirroring what we observed following G007-LK treatment of Apc^{Min} mice, genetic TNKS1/2 suppression did not block Apc^{Min}-driven tumor growth. Both Apc^{Min}/sh*Ren* and Apc^{Min}/sh*Tnks* mice developed highly proliferative colonic and small-intestinal tumors with minimal evidence of differentiation (Fig. 2C; Supplementary Fig. S3B). Accordingly, Apc^{Min}/sh*Ren* and Apc^{Min}/sh*Tnks* mice showed no significant difference in relative tumor area, hematocrit, or survival (Fig. 2D–F).

The *in vivo* data described above highlights that response to TNKS inhibition may be dependent on the genetic context of the tumor. We sought to reconcile which model better reflects the biology and therapeutic response of human colorectal cancer; therefore, we analyzed two independent clinical datasets (MSK-IMPACT colorectal and The Cancer Genome Atlas PanCan colorectal cancer) for the type and frequency of APC mutations. Consistent with previous analyses (1, 2), APC mutations were present in 1,231/1,693 (73%) patient samples, with predominantly nonsense mutations throughout the N-terminal half of the gene (Fig. 3A). Further examination of tumors with two identifiable APC mutations revealed striking selection for cancers carrying at least one truncating mutation within the mutation cluster region (MCR) that spans amino-acid residues approximately 1,250 to 1,580 (Fig. 3B). Moreover, cases in which only one allele could be identified showed a further bias toward mutations in the MCR (Supplementary Fig. S4A and S4B). These observations are consistent with previous analyses of an independent cohort (21), and strongly imply that accurate genetic models of human colorectal cancer should harbor at least one MCR mutation in APC, more C-terminal than either the Apc^{Min} or Apc^{Flox} alleles (Fig. 3B).

To engineer defined nonsense mutations both preceding and within the MCR, we used recently described optimized base editing tools (22). We transfected WT C57BL/6 intestinal organoids with the FNLS base-editing enzyme (22), and single-guide RNAs (sgRNA) targeting codons Q884 (Apc^{Q884X}) and Q1405 (Apc^{Q1405X}; Fig. 3C; Supplementary Fig. S5A and S5B). The Q884X mutation closely mimics the R876X allele

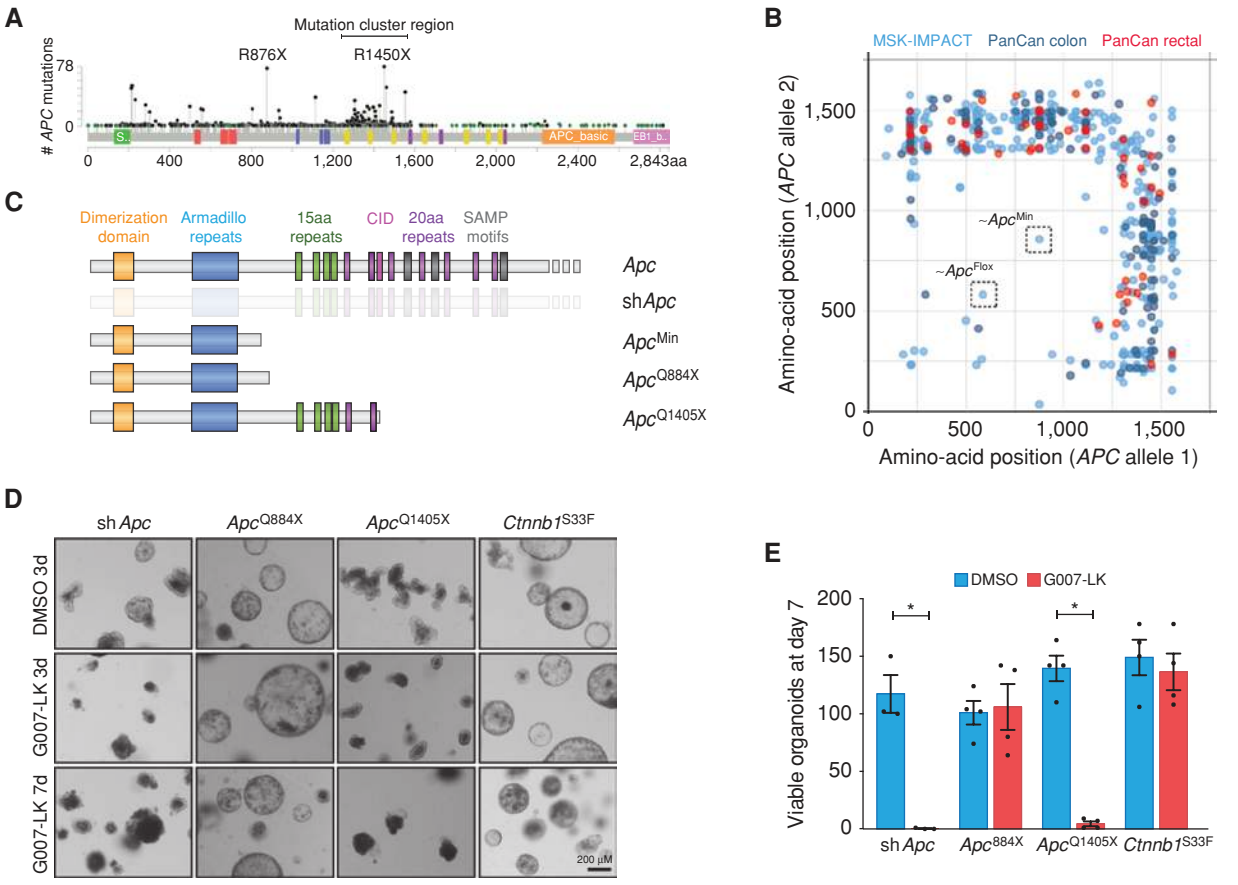

Figure 3. An MCR truncation in APC sensitizes organoids to TNKS1/2 blockade. **A,** Lollipop plot of publicly available human colorectal cancer MSK-IMPACT and PanCan data showing mutation frequency across all codons in APC. **B,** Scatter plot of MSK-IMPACT and PanCan data from colorectal cancers carrying two distinct mutations in *APC* highlights the presence of late truncating mutations in most colorectal cancers. **C,** APC mutations generated in organoids. **D,** Brightfield images of APC-mutant or βCAT^{S33F} organoids treated with DMSO or G007-LK (1 µmol/L) as indicated. **E,** Quantitation of viable organoids after 7 days of DMSO or G007-LK treatment ($n = 3$–4, error bars = SEM, *, $P < 0.05$, unpaired t test with Welch correction). All organoids were passaged once at day 3. (*continued on next page*)

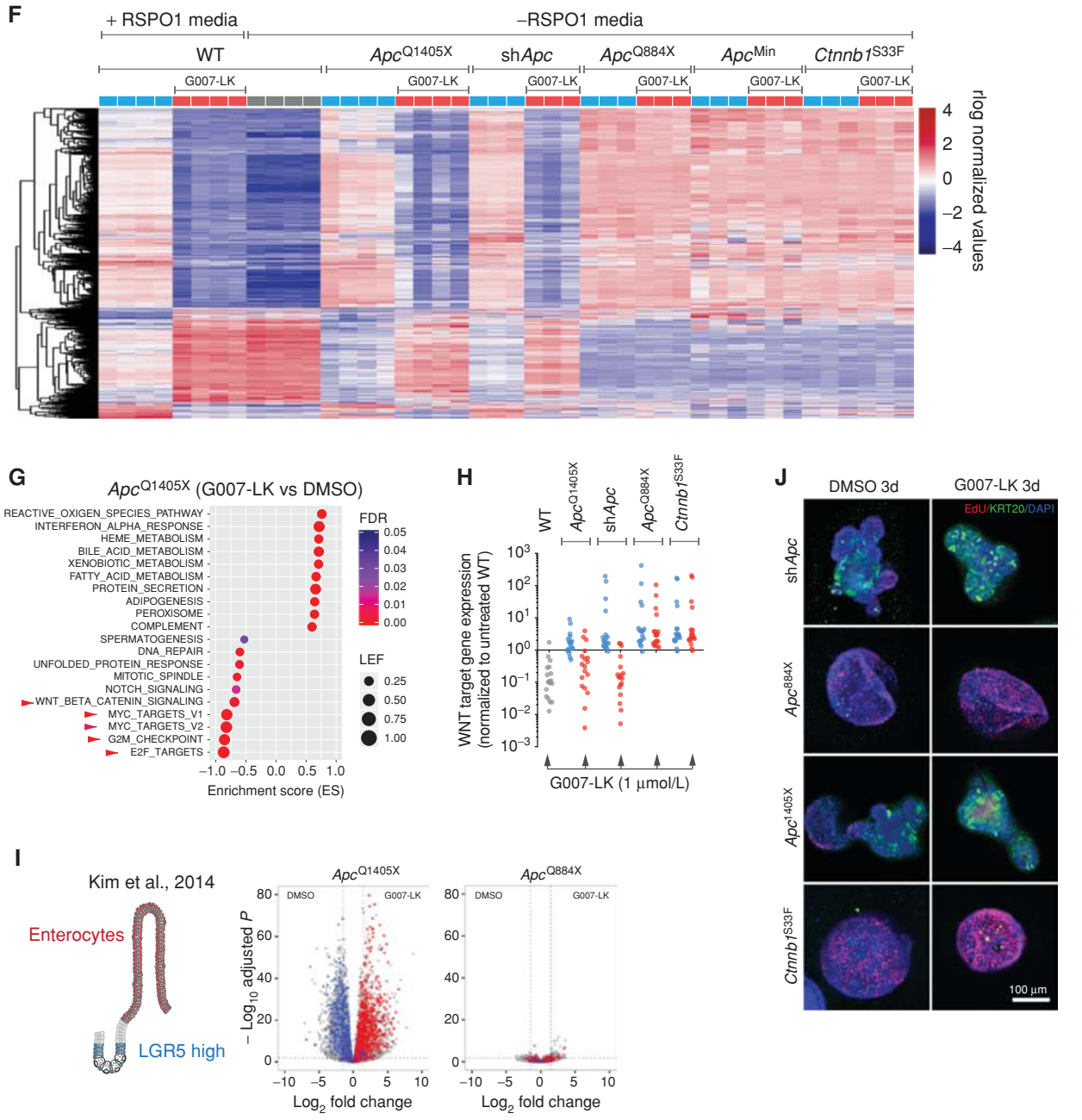

Figure 3. ***(Continued)*** **F,** Heat map representing relative gene expression in WT, *Apc*, and *Ctnnb1*^{S33F} organoids cultured in DMSO or G007-LK for 3 days. Shown are 1,472 genes with a $\log_2$FC > 2 and $P_{adj} < 0.01$ in G007-LK–treated WT organoids, compared with DMSO controls. **G,** Summary plot of GSEA results, including 10 significantly positively and negatively enriched gene sets in G007-LK–treated *Apc*^{Q1405X} organoids. Leading-edge fraction (LEF) is the fraction of genes in the gene set included in the leading edge of the GSEA plot. **H,** Mean expression of 18 validated WNT target genes (Supplementary Table S2) following 3 days of treatment with G007-LK or DMSO, normalized to DMSO-treated WT organoids. **I,** Schematic depiction of the cell populations identified by gene signatures in Kim and colleagues (2014; ref. 28). Adjacent color-coded volcano plots of G007-LK–treated *Apc*^{Q1405X} and *Apc*^{Q884X} organoids highlight genes included in these signatures. Genes upregulated following G007-LK treatment are shifted to the right. **J,** Immunofluorescence staining of *Apc*-mutant or *Ctnnb1*^{S33F} organoids cultured in DMSO or G007-LK (1 μmol/L) for 3 days. Organoids were pulsed with EdU for 4 hours to label proliferative cells.

seen in human colorectal cancers, which truncates APC after the armadillo repeats, but before the first set of 15 amino acid β-catenin–binding repeats (Fig. 3C). Truncation of APC at Q1405, immediately after the second 20 amino acid repeat (20AAR), removes a conserved "catenin inhibitory domain" (CID; Fig. 3C) that is thought to be critical for proper β-catenin regulation (23, 24). Indeed, studies in *Drosophila*, cancer cell lines, and mice have shown this allele promotes high levels of WNT activation (23–26). In addition to engineered *Apc* mutations, we generated *Apc*^{Min} and sh*Apc* organoids, as well as those with an activating missense mutation in serine residue 33 of *Ctnnb1* (βCAT^{S33F}; Supplementary Fig. S5B); this mutant

protein cannot be phosphorylated at S33 by GSK3β, and is therefore independent of the DC.

All mutant organoids could be maintained in the absence of WNT/RSPO ligands, confirming cell-intrinsic constitutive activation of WNT signaling. To assess the response to TNKS inhibition, we treated each mutant with G007-LK (1 μmol/L) for 7 days, and quantified cell survival by counting viable organoids. As expected, βCAT^{S33F} organoids showed no change in morphology or viability following G007-LK treatment. Similarly, and consistent with the lack of response in APC^{Min} cells, APC^{Q884X} organoids showed no response to G007-LK. In contrast, APC^{Q1405X} and sh*Apc* organoids showed reduced crypt branching after 3 days, and were unable to survive 7 days of G007-LK treatment (Fig. 3D and E). Importantly, the lack of response to TNKS inhibition in APC^{Q884X} and APC^{Min} cultures was not specific to these similar truncated proteins, as organoids carrying an even earlier truncation, APC^{Δ580} (generated from the *Apc*^{Flox} allele; ref. 27), were also resistant to G007-LK treatment (Supplementary Fig. S6A). Furthermore, the effect was not specific to G007-LK, as we noted a similar genotype-dependent response with two independent TNKS inhibitors of different chemotypes: NVP656 (20) and XAV939 (ref. 6; Supplementary Fig. S6B).

To gain insight into the molecular events underlying the genotype-dependent response to G007-LK, we performed transcriptome profiling by RNA sequencing (RNA-seq). We treated WT, *Apc*-mutant (*Apc*^{Min}, *Apc*^{Q884X}, *Apc*^{Q1405X}, and sh*Apc*), and *Ctnnb1*-mutant (βCAT^{S33F}) organoids with 1 μmol/L G007-LK (or DMSO vehicle) for three days and recovered cells for mRNA sequencing. Principal component analysis of the data revealed tight clustering of individual biological replicates of similar genotypes, but broad gene-expression differences between organoid groups (Supplementary Fig. S7A). More than 80% of the variance in gene expression between groups was accounted for by PC1, which included a number of canonical WNT target genes, including *Sox17, Nkd1, Wnt6*, and *Prox1*. In general, organoids with βCAT^{S33F} mutations and early APC truncations clustered together and had higher WNT target gene expression, whereas *Apc*^{Q1405X} and sh*Apc* organoids had lower WNT target induction, albeit markedly higher than WT organoids (Supplementary Fig. S7B). Importantly, the transcriptome analysis showed that organoids derived from *Apc*^{Min} mice (*Apc*^{L850X}) and those with a similar base editing–induced mutation (*Apc*^{Q884X}) had highly similar global gene-expression patterns (Fig. 3F; Supplementary Fig. S7A), highlighting the fidelity of base editing for modeling specific genetic alleles in organoids.

Treatment with G007-LK did not dramatically alter global gene expression of *Ctnnb1*^{S33F}, *Apc*^{Min}, and *Apc*^{Q884X} cultures, but caused a striking shift in the transcriptome of sh*Apc*, *Apc*^{Q1405X}, and WT organoids. Indeed, significant gene-expression changes ($\log_2$FC >2, P_{adj} <0.01) observed in WT cultures following treatment with G007-LK (or RSPO1 withdrawal) were closely mirrored in sh*Apc* and *Apc*^{Q1405X} organoids (Fig. 3F). In contrast, few transcriptional changes were observed in G007-LK–treated *Apc*^{Min} and *Apc*^{Q884X} organoids (28 and 56 genes, respectively; $\log_2$FC >2, P_{adj} < 0.01), and there were zero (0) significant changes in gene expression observed in βCAT^{S33F} cultures (Supplementary Table S1). The profound lack of response in βCAT^{S33F} organoids strongly suggests that the primary effect of TNKS inhibition is modulating DC activity via AXIN1/2.

Gene set enrichment analysis (GSEA) of G007-LK–treated *Apc*^{Q1405X} organoid transcriptomes identified an upregulation of networks related to differentiated intestine function, such as protein and lipid metabolism, and a decrease in cell cycle–related MYC and E2F targets (Fig. 3G). Conversely, MYC-related gene sets were actually enriched in G007-LK–treated *Apc*^{Q884X} cells (Supplementary Fig. S7C). As expected, G007-LK also induced a significant decrease in WNT/β-catenin signaling in *Apc*^{Q1405X} organoids (Fig. 3H; Supplementary Table S2), whereas WNT signaling was not significantly altered in *Apc*^{Q884X}, *Apc*^{Min}, or *Ctnnb1*^{S33F} G007-LK–treated organoids (Fig. 3H). We next compared our data to two published, experimentally derived intestinal gene signatures that distinguish crypt-based stem cells and differentiated enterocytes (28, 29). In both cases, genes linked with terminal enterocyte differentiation were strongly upregulated following treatment of *Apc*^{Q1405X} organoids with G007-LK, whereas genes associated with LGR5-positive stem cells were downregulated (Fig. 3I; Supplementary Figs. S7D and S8). Consistent with the transcriptional changes, G007-LK–treated sh*Apc* and *Apc*^{Q1405X} organoids showed rapid cell-cycle arrest and induction of differentiation markers (KRT20 and alkaline phosphatase; Fig. 3J; Supplementary Fig. S9A and S9B). No apparent increase in differentiation or loss of stem-cell identity were observed following treatment of *Apc*^{Q884X} or *Ctnnb1*^{S33F} organoids (Fig. 3I and J; Supplementary Figs. S7–S9). The organoid response to G007-LK was not a transient cell-cycle arrest, but likely reflects an enterocyte differentiation program, as organoid survival at 7 days was only slightly improved following washout of the drug after 3 days of treatment (Supplementary Fig. S10A and S10B). Furthermore, the intestinal differentiation response observed in organoids is consistent with what we observed following G007-LK treatment of sh*Apc* tumors *in vivo* (Fig. 1) or genetic APC restoration (4). In all, these data support the notion that TNKS inhibition reengages endogenous WNT regulation and normal intestinal differentiation in cells carrying a late APC truncation, closely mimicking the effect APC restoration (4).

To determine whether similar a genotype-dependent response was apparent in human colorectal cancer cells, we used a well-characterized human colorectal cancer cell line (DLD1) that carries a late truncating allele of *APC*^{1417X} and shows a marked WNT transcriptional response to TNKS inhibitors. Using Cas9 and an sgRNA analogous to the *Apc*^{Q884X} guide used in the mouse studies (*APC*^{Q883}), we created multiple independent DLD1 lines with shorter APC truncations (Fig. 4A; Supplementary Fig. S11A). Consistent with what we observed in mouse organoids, the WNT-suppressive response of G007-LK was abrogated in *APC*^{Q883} cells (Fig. 4B). Similarly, patient-derived human colorectal cancer organoids (30) carrying late truncating mutations in APC showed decreased WNT target gene (*LGR5* and *AXIN2*) expression after 3 days of G007-LK treatment (Fig. 4C; Supplementary Fig. S11B and S11C). Together, these data show that TNKS inhibitors can suppress WNT targets in human colorectal cancer cells carrying MCR APC truncations.

Our cellular and transcriptome analyses demonstrate that *Apc*^{Q1405X} organoids show profound WNT pathway downregulation in response to TNKS1/2 inhibition. Indeed, *Apc*^{Q1405X} organoids showed a marked decrease in nonphosphorylated (active) β-catenin following treatment with G007-LK

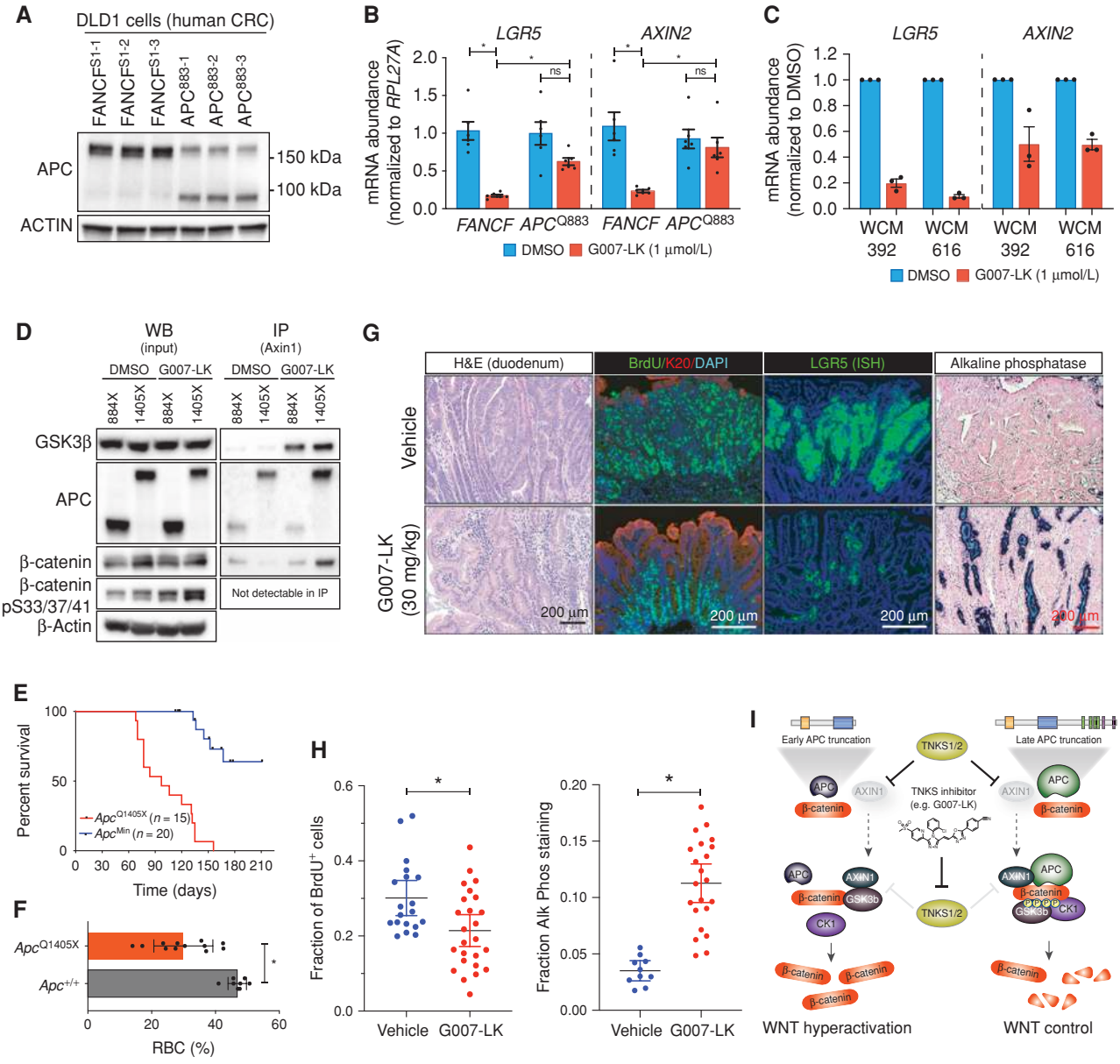

Figure 4. Human cells and Apc^{Q1405X} mouse adenomas with MCR truncations respond to TNKS1/2 inhibition. **A,** Western blot of DLD1 cells expressing Cas9, transduced with sgRNAs targeting either *FANCFS1* (negative control) or *APC* (near codon Q883). Targeting with the *APC* sgRNA generated a shorter truncated protein. **B,** Expression of WNT target genes *LGR5* and *AXIN2* in *FANCFS1* or APC^{Q883} transduced DLD1s following 72-hour treatment with G007-LK, as indicated. **C,** Expression of WNT target genes *LGR5* and *AXIN2* in patient-derived organoids following 72-hour treatment with G007-LK, as indicated. Raw values of individual replicate experiments are presented in Supplementary Fig. S11. **D,** Immunoprecipitation (IP) of AXIN1 in whole-cell lysates from Apc^{Q1405X} and Apc^{Q884X} cells treated with G007-LK or DMSO for 24 hours. WB, Western blot. **E,** Kaplan–Meier plot showing survival of Apc^{Q1405X} mice (red line) as compared with Apc^{Min} mice (blue line). **F,** Bar graph showing hematocrit from $Apc^{Q1405X/+}$ and $Apc^{+/+}$ mice at 10–11 weeks. **G,** IHC, immunofluorescence, and *in situ* hybridization (LGR5) stains from the proximal small intestine of 10-week-old Apc^{Q1405X} mice treated with vehicle or G007-LK (30 mg/kg, once daily) for one week. Apc^{Q1405X} mice treated with G007-LK show a differentiation profile marked by decreased BrdU incorporation, decreased *Lgr5* abundance, and increased alkaline phosphatase staining. **H,** Quantitation of the fraction of BrdU-positive cells (left) and alkaline phosphatase–positive area (right) in individual tumors ($n = 3$–6 tumors/mouse; $n = 3$–6 mice/treatment). Bars represent mean and 95% CI. **I,** Model for data presented, indicating that late truncating mutations in APC, but not early truncating mutations, can engage the destruction complex in response to TNKS1/2 inhibition. Subsequent DC assembly reestablishes normal control of WNT signaling.

(Supplementary Fig. S12A). To directly test whether this was due to increased activity of the DC, we measured physical association of key DC members by immunoprecipitation of AXIN1. To produce the cell numbers required for effective immunoprecipitation, we generated 2-D cell lines carrying $Kras^{G12D}$ and *Trp53*-null mutations and either Apc^{Q884X} or APC^{Q1405X} truncations.

Baseline AXIN1 levels were higher in Apc^{Q884X} cells, but as expected, G007-LK treatment drove AXIN1 stabilization in both contexts (Supplementary Fig. S12B and S12C). The shorter APC^{Q884X} mutant protein was more abundant than APC^{Q1405X} in intestinal cells; however, AXIN1 selectively associated with the longer truncated form (Fig. 4D). G007-LK

treatment further strengthened this binding and enabled increased association with β-catenin. Consistent with this, G007-LK–treated Apc^{Q1405X} cells showed increased phosphorylation of β-catenin at S33/S37/T41 (Fig. 4D). We were unable to detect phosphorylated β-catenin in AXIN1 IPs, likely due to the rapid release of phospho-β-catenin from this complex. In contrast to APC^{Q1405X}, APC^{Q884X} mutant protein showed no increased binding to AXIN1 in the presence of G007-LK, did not enable further β-catenin association, and produced only a minor increase in $βCAT^{S33}$ phosphorylation (Fig. 4D).

Our organoid data described above indicate that the position of APC truncations dictates response to TNKS1/2 inhibition. To directly test this hypothesis *in vivo*, we generated a new Apc^{Q1405X} mouse allele by direct base editing in C57BL/6 zygotes (see Methods for detail). Sanger sequencing of DNA from viable founder mice confirmed the expected C>T transition in 14 of 30 (47%) animals, with the remaining mice showing a mixture of non-C>T changes, indels, and WT sequence (Supplementary Table S3). As expected, no $Apc^{Q1405X/Q1405X}$ founder mice were obtained, due to early embryonic lethality of homozygous APC mutants (31), whereas Apc^{Q1405X} heterozygous mice became moribund by 12 to 14 weeks of age (median survival: 97 days; Fig. 4E). As commonly observed in other APC-mutant models, early-onset anemia correlated with multifocal adenoma growth throughout the small intestine (most likely following LOH, as occurs in Apc^{Min}; ref. 18; Fig. 4F and G).

To determine whether established Apc^{Q1405X} adenomas were sensitive to TNKS1/2 inhibition, we treated tumor-bearing 10-week-old $Apc^{Q1405X/+}$ mice with G007-LK (30 mg/kg, once daily) or vehicle for 1 week. Histologic sections of G007-LK–treated intestinal tumors showed decreased nuclear to cytoplasmic ratio, nuclear polarization, and a transition to differentiated villi-like structures (Fig. 4E, G, and H). Consistent with this, immunofluorescent staining showed reduced proliferation (Fig. 4G and H, BrdU) and induction of differentiation markers (Fig. 4G and H, KRT20 and ALPi). In contrast to treated Apc^{Min} polyps, LGR5 expression was dramatically reduced in Apc^{Q1405X} lesions, confirming reduced WNT signaling within the adenoma (Fig. 4G, LGR5). Together, this data supports our findings in organoids that truncating mutations in the MCR of APC render cells sensitive to WNT suppression via TNKS inhibition (Fig. 4I).

DISCUSSION

We previously reported that restoring APC expression induces sustained tumor regression in colorectal cancer (4). Here, using genetically defined animal models, organoids, and human cell lines, we show that TNKS inhibition can reengage the same endogenous tumor-suppressive mechanism, but this molecular switch is highly dependent on the specific APC disruption. Tumor cells containing "early" truncating mutations that eliminate all identified AXIN1/2 and β-catenin motifs (e.g., Apc^{Min}, Apc^{Q884X}) do not respond to TNKS inhibition, yet those with an MCR mutation can regulate β-catenin and suppress oncogenic signaling in response to AXIN1/2 stabilization. To our knowledge, this is the first *in vivo* demonstration that subtle changes in colorectal cancer–initiating genetic events can lead to profound changes in response to targeted therapy, and it has implications for strategies that aim to modulate WNT activity through the DC.

Consistent with previously published data (21), we observed in three independent datasets that the majority of colorectal cancers carry at least one nonsense mutation within the MCR amino acid residues (~1,250–1,580). This mutational pattern is hypothesized to be a selection for mutations that enable oncogenic transformation yet retain partial β-catenin regulation, providing a "just right" level of WNT activation (32–34). Interestingly, APC structure–function studies in colorectal cancer cell lines and model organisms suggest that truncations at Q1405 that remove the CID immediately after the second 20AAR disrupt β-catenin turnover, and thus drive high levels of WNT activation (23, 24). Consistent with this, our Apc^{Q1405X} organoids, carrying the same truncating allele, hyperactivate WNT signaling, and heterozygous $Apc^{Q1405X/+}$ mice develop intestinal tumors with 100% penetrance. However, in response to TNKS inhibition, APC^{Q1405X} can engage the DC to suppress hyperactive WNT signaling; this response would not have been predicted from structure–function models. It is important to note that although most human colorectal cancers harbor both an early and late truncation, and our organoids were engineered to carry two Apc^{Q1405X} alleles, we observed that one of the biological replicates (replicate A) carried an unexpected heterozygous deletion in one allele of *Apc* (Supplementary Fig. S13A–S13C). Although these cells express only one truncated allele and show moderately higher baseline WNT activity, they have an identical response to TNKS inhibition (Supplementary Fig. S13D), implying that the presence of one MCR-truncated allele is sufficient to engage the DC.

Given the importance of APC interaction with β-catenin and the DC, it is somewhat counterintuitive that sh*Apc* organoids and tumors show such robust WNT suppression and differentiation responses to G007-LK, despite extremely potent knockdown (Supplementary Fig. S14). We propose that the reason underlying the response of sh*Apc* cells is the presence of a minimal residual amount of full-length APC protein that can be detected in complex with AXIN1, but not in whole-cell lysates (Supplementary Fig. S14). Although the amount of APC is dramatically reduced, the residual protein contains all β-catenin and AXIN binding domains that allow it to effectively engage the DC and, following AXIN stabilization, drive WNT suppression. The observation that only minimal full-length APC protein is required for tumor suppression is consistent with our previously published work, which showed that intestinal adenomas have a phenotypic response to genetic APC restoration even before APC protein is detectable by Western blot analysis (4).

In all, these findings highlight that distinct mutations within the same gene can appear phenotypically similar (hyperactive WNT) but have profoundly different biochemical responses to therapies targeting their mechanism of action. This reinforces the need to create accurate and representative genetic models for understanding the molecular events of disease and therapy response.

Our results contrast with recent *in vitro* work, which concluded that cells with early APC truncations are uniquely sensitive to TNKS inhibition (19). In our experiments, WNT suppression correlated precisely with cell-cycle arrest and differentiation, consistent with the role of WNT as a driver of

self-renewal and tumorigenesis. In contrast, although almost all cell lines assessed by Tanaka and colleagues showed WNT suppression following TNKS inhibition, most were not dependent on WNT for survival, and thus were classified as resistant (19). We believe it is likely that either the accumulation of specific oncogenic events or prolonged *in vitro* culture relieved their WNT dependence, confounding the correlation of TNKSi response and APC/WNT alterations. Indeed, one recent study in lung adenocarcinoma demonstrated that WNT/RSPO-dependent 3-D organoid cultures become WNT-independent when cultured in 2-D (35). Furthermore, Lord and colleagues recently proposed that activating KRAS mutations may correlate with resistance to TNKS inhibitors (36). Although the latter study did not ascribe a specific mechanism to this possible interaction, it is consistent with multiple observations that concurrent inhibition of classic oncogenic signaling pathways such as MAPK or AKT enhances the response to TNKS inhibition (12, 20, 37–39).

Although TNKS inhibition is unlikely to be used as a monotherapy for cancer treatment, it is perhaps worth (re) considering its utility in patients with familial adenomatous polyposis (FAP), who most commonly carry heterozygous germline mutations in the MCR (40) and ultimately have few options other than surgical removal of the colon. Our data imply that FAP-associated adenomas may respond to TNKS inhibitors, although a number of issues of drug dose, bioavailability, and safety would need to be addressed before they could be considered a viable option.

Understanding how specific oncogenic insults drive cell transformation and affect therapy response is a key goal of precision oncology medicine. WNT pathway hyperactivation is a clear cancer driver in a number of malignancies, including colorectal cancer (1, 4, 41, 42), and has been suggested as an immune-modulator that may affect response to checkpoint inhibitors (43–45). Although WNT-targeted agents have yet to make significant progress in clinical medicine, approaches to block WNT hyperactivation are of keen interest for cancer treatment. Defining the genetic contexts in which they will be effective, as described here, is critical for the future development and application of WNT-targeted therapeutics.

METHODS

Cloning

Individual *Tnks* and *Tnks2* shRNAs were cloned into an MLPE vector at *Xho*I and *Eco*RI sites as described previously (46). For tandem shRNA cloning, the destination vector containing shRNA #1 was digested with *Eco*RI for 4 hours at 37°C and incubated with CIP for 30 minutes at 37°C. shRNA #2 was PCR-amplified using miRE-TX_For and miRE_*Eco*RI_Rev primers (Supplementary Table S4). Positive clones were identified by restriction digest and validated by Sanger sequencing with mir30_seq primer (Supplementary Table S4). Tandem shRNA cassettes were shuttled into the col1A1 targeting vector (cTGME) following PCR amplification with miRE_*Xho*I_For and miRE_*Eco*RI_Rev primers, and *Xho*I/*Eco*RI digest. For the shRNA sensor assay, shRNA target sequences against *Tnks* and *Tnks2* were arrayed, produced as a synthetic gBlock (IDT), and cloned into the 3′UTR of a dTomato sensor vector (*Xho*I/*Eco*RI). For *Tnks*- or *Tnks2*-specific sensors, gBlocks with only *Tnks* or *Tnks2* target sequences were designed and cloned as described above. sgRNA cloning into the vector LRT2B cloning was performed as described previously (22, 47). The shApc.2235E retroviral vector used to transduce organoids was generated by Gibson cloning into the pMSCV-rtTA3-miRE vector.

Mutation Detection by T7 Assay

Cas9-induced mutations were detected using the T7 endonuclease I (NEB). Briefly, the target region surrounding the expected mutation site was PCR-amplified using Herculase II (600675, Agilent Technologies). PCR products were column-purified (Qiagen) and subjected to a series of melt–anneal temperature cycles with annealing temperatures gradually lowered in each successive cycle. T7 endonuclease I was then added to selectively digest heteroduplex DNA. Digest products were visualized on a 2.5% agarose gel.

Cells

HEK293T (ATCC CRL-3216) and DLD1 cells (ATCC CCL-221) were purchased from ATCC and maintained in DMEM (Corning) supplemented with 10% (v/v) FBS, at 37°C with 5% CO_2. NIH/3T3 cells (ATCC CRL-1658) were maintained in DMEM (Corning) supplemented with 10% (v/v) bovine calf serum. Cells were regularly tested for *Mycoplasma* using the MycoAlert Mycoplasma Detection Kit (Lonza, #LT07-418) and discarded if found positive.

Virus Production

HEK-293T cells cultured in DMEM + 10% FBS were cotransfected with retroviral vector, CMV-Gag-Pol, CMV-Eco envelope, and pcSUPER-shPasha (to prevent miRNA processing of the nascent retroviral RNA transcript). Cells were washed 12 to 24 hours after transfection, and viral supernatants were collected from 36 to 60 hours post-transfection. Detailed protocol available at: http://www.dowlab.org/protocols. For LRT2B-sgRNA virus, no pcSUPER-shPasha was included.

shRNA Sensor Assay

The sensor assay was adapted (48) using NIH-3T3s, which were cultured in DMEM + 10% calf serum. Following transduction, the top 20% brightest dTomato-positive cells were collected by FACS. Sorted cells were subsequently transduced with shRNA virus at 1:10 to achieve approximately single multiplicity of infection. Five days post-infection, dTomato expression was measured by flow cytometry, and knockdown was calculated as relative decrease from parental population after subtraction of background signal.

Human Colorectal Cancer Cell Lines and Patient-Derived Organoids

DLD1 cells were transduced with lentivirus expressing Cas9 (Addgene #110837), in the presence of hexadimethrine bromide (Polybrene; 8 μg/μL). Two days after transduction, cells were selected in puromycin (2 μg/mL). DLD-Cas9 cells (1×10^4) were plated in a 6-well plate and transduced with the LRT2B vector (Addgene #110854) containing either hAPC.884 or FANCF.S1 control sgRNAs. Two days after transduction, cells were selected in blasticidin S (5 μg/mL) and 0.3×10^4 LRT2B-transduced cells were plated for treatment with either DMSO or G007-LK (1 μmol/L) for 3 days for RNA and protein collection. Deidentified, patient-derived human colorectal cancer organoids (WCM392 and WCM616; described previously; ref. 30) were obtained from the Institute for Precision Medicine at Weill Cornell Medicine (New York, NY). Organoids were cultured in Basal Media + B27, and treated with either DMSO or G007-LK (1 μmol/L) for 3 days.

ES Cell Targeting

Embryonic stem (ES) cells were maintained on irradiated feeders; C57BL/6 cells were cultured 2i media and KH2 cells were cultured in M15 media, both containing LIF as outlined previously (46). Cells were transfected with targeting vector and *CAGs-FlpE* vector using a Lonza X Unit Nucleofector with P3 buffer kit (Lonza #V4XP-3032). Two days

following transfection, cells were treated with media containing 150 μg/mL hygromycin, and individual surviving clones were picked after 9 to 10 days of selection. Two days after clones were picked, hygromycin was removed from the media, and cells were cultured in standard M15 thereafter. To confirm single-copy integration at the *col1a1* locus, we first validated expected integration by multiplex *col1a1* PCR (3) and then confirmed the presence of a single GFP cassette using the TaqMan copy-number assay, according to the manufacturer's instructions (Invitrogen).

Isolation and Culture of Intestinal Organoids

Isolation, maintenance, and staining of mouse intestinal organoids has been described previously (49, 50). Briefly, for isolation, 15 cm of the proximal small intestine was removed and flushed with cold PBS. The intestine was then cut into 5-mm pieces, vigorously resuspended in 5 mmol/L EDTA-PBS using a 10-mL pipette, and placed at 4°C on a benchtop roller for 10 minutes. This was then repeated for a second time for 30 minutes. After repeated mechanical disruption by pipette, released crypts were mixed with 10 mL DMEM Basal Media [Advanced DMEM/F12 containing penicillin/streptomycin, glutamine, 1 mmol/L *N*-acetylcysteine (Sigma Aldrich A9165-SG)] containing 10 U/mL DNAse I (Roche, 04716728001), and filtered sequentially through 100-μm and 70-μm filters. FBS (1 mL; final 5%) was added to the filtrate and spun at 1,200 rpm for 4 minutes. The purified crypts were resuspended in basal media and mixed 1:10 with Growth Factor Reduced (GFR) Matrigel (BD Biosciences, 354230). Forty microliters of the resuspension was plated per well in a 48-well plate and placed in a 37°C incubator to polymerize for 10 minutes. Small intestinal organoid growth media (250 μL basal media containing 50 ng/mL EGF (Invitrogen PMG8043), 100 ng/mL Noggin (PeproTech 250-38), and 500 ng/mL R-spondin (R&D Systems, 3474-RS-050, or from conditioned media) was then laid on top of the Matrigel. Where indicated, doxycycline was added to experiments at 500 ng/mL.

For subculture and maintenance, media were changed on organoids every two days and they were passaged 1:4 every 5 to 7 days. To passage, the growth media was removed and the Matrigel was resuspended in cold PBS and transferred to a 15-mL Falcon tube. The organoids were mechanically disassociated using a P1000 or a P200 pipette and pipetting 50 to 100 times. Seven milliliters of cold PBS was added to the tube and pipetted 20 times to fully wash the cells. The cells were then centrifuged at 1,000 rpm for 5 minutes and the supernatant was aspirated. The cells were then resuspended in GFR Matrigel and replated as above. For freezing, after spinning the cells were resuspended in basal media containing 10% FBS and 10% DMSO and stored in liquid nitrogen indefinitely.

Organoid Transfection

Murine small intestinal organoids were cultured in transfection medium containing CHIR99021 (5 μmol/L) and Y-27632 (10 μmol/L) for 2 days prior to transfection. Single-cell suspensions were produced by dissociating organoids with TrypLE Express (Invitrogen #12604) for 5 minutes at 37°C. After trypsinization, cell clusters in 300 μL transfection medium were combined with 100 μL DMEM/F12–Lipofectamine 2000 (Invitrogen #11668)–DNA mixture (97 μL–2 μL–1 μg), and transferred into a 48-well culture plate. The plate was centrifuged at 600 × *g* at 32°C for 60 minutes, followed by another 6-hour incubation at 37°C. The cell clusters were spun down and plated in Matrigel. For selecting organoids with APC mutants, exogenous R-spondin1 and Noggin were withdrawn 2 days after transfection.

Organoid Drug Treatment and Counts

Organoids were plated in 100 μL Matrigel (2 × 50 μL droplets) in one 12-well plate and cultured in Advanced DMEM/F12 + EGF media with either DMSO or G007-LK (1 μmol/L). Three days after plating, 8 brightfield images were taken in a vertical line, approximately the length of one droplet. Images were then compiled in one document, and viable organoids were counted for each condition. Organoids were then passaged either 1:2 or 1:1 (based on confluency) and then cultured again in DMSO or G007-LK. Day 7 counts were calculated from brightfield images and multiplied by the passaging factor.

EdU Flow Cytometry

Organoid EdU flow cytometry was performed using the Click-iT Plus EdU Alexa Fluor 647 Flow Cytometry Assay Kit (Thermo Fisher Scientific, # C10634). Organoids were first incubated with 10 μmol/L EdU for 4 hours at 37°C. One well of a 12-well plate was broken up by pipetting vigorously 50 times in 1 mL PBS, then diluted in 5 mL of PBS. Cells were pelleted at 1,100 rpm × 4 minutes at 4°C, then resuspended in 50 μL TrypLE and incubated at 37°C for 5 minutes. Five milliliters of PBS was then added to inactivate the TrypLE, and cells were pelleted. Cells were resuspended in 250 μL of 1% BSA in PBS, transferred to a 1.7-mL tube, and then pelleted at 3,000 rpm × 4 minutes. Cells were then resuspended in 100 μL Click-iT fixative, and processed as instructed in the Click-iT Plus EdU protocol (starting with Step 4.3). Wash and reaction volumes were 250 μL.

Animal Studies

Production of mice and all treatments described were approved by the Institutional Animal Care and Use Committee (IACUC) at Weill Cornell Medicine, under protocol number 2014-0038. ES cell–derived mice were produced by blastocyst injection, and animals were either maintained on a mixed C57B6/129 background for experimental breeding or back-crossed to C57BL/6N mice. Progeny of both sexes were used for experiments and were genotyped for specific alleles (*Lgr5-GFP-IRES-CreER, CAGs-rtTA, Col1A1, TG-shApc.2235E, TG-Ren.713, TG-shTnks1/2-3341-1328, TG-shTnks1/2-1385-3004, Apc*^{Q1405X}, and *Apc*^{Min}) using primers described in Supplementary Table S3 and protocols available at http://www.dowlab.org/protocols. Production of mice and all treatments described were approved by the IACUC at Weill Cornell Medicine under protocol number 2014-0038. For induction of the CreER transgene, animals were administered 4OHT (25 mg/kg in 90% v/v corn oil, 10% v/v ethanol) via intraperitoneal injection. Where required, doxycycline was administered via food pellets (200 mg/kg; Harlan Teklad) from 6 to 8 weeks of age. For G007-LK treatment studies, G007-LK (30 mg/kg, MedChemExpress) was mixed with 20% CremaphorEL and 70% PBS, then delivered by daily intraperitoneal injection. Mice were sacrificed after 7 or 14 days. Animal studies were not blinded during treatment; however, quantitation of tumor burden involved measurements by two parties, one blinded to the treatment groups.

Immunofluorescence and In Situ Hybridization

Tissue, fixed in freshly prepared 4% paraformaldehyde for 24 hours, was embedded in paraffin, and sectioned by IDEXX RADIL. Sections were rehydrated and unmasked (antigen retrieval) by heat treatment for 5 minutes in a pressure cooker in 10 mmol/L Tris/1 mmol/L EDTA buffer (pH 9) containing 0.05% Tween 20. Sections were blocked in TBS/0.1% Triton X-100 containing 1% BSA. Organoids were stained as described previously (50), with the following exception: Prior to beginning the EdU/Keratin20 staining, organoids were washed once with 300 μL PBS, then incubated with 300 μL Cell Recovery Solution for 20 minutes on ice. Primary antibodies used were: rabbit anti-KRT20 (1:200, Cell Signaling Technology, #13063), rat anti-BrdU (1:200, Abcam #ab6326). Secondary antibodies were applied in TBS for 1 hour at room temperature in the dark, washed twice with TBS, counterstained for 5 minutes with DAPI and mounted in ProLong Gold (Life Technologies, #P36930). Secondary antibodies used were: anti-rabbit 488 (1:500, Abcam, #ab150073) and anti-rat 594 (1:500, Abcam, #ab150156). Intestinal alkaline phosphatase staining was performed using the BCIP/NBT Alkaline Phosphatase (AP) Substrate Kit

(Vector Laboratories, #SK-5400; 1 drop lemavisole solution/5 mL was added prior to the reaction to inhibit endogenous alkaline phosphatase activity; Vector Labs, #SP-5000) and counterstained with Nuclear Fast Red (Sigma-Aldrich, #60700). For LGR5 ISH, freshly cut 5-μm paraffin sections were stained using RNAscope 2.5 LS RED Kit (ACD, catalog no. 322150) and Bond Polymer Refine Red Detection Kit (Leica, catalog no. DS9390) on a Leica Bond RX instrument following routine manufacturer's protocol ACD 2.5 Red. RNAscope 2.5 LS probes for Ms-LGR5 (ACD, catalog no. 312178). DapB-negative control (ACD, catalog no. 312038) was used with hybridization at 42°C for 2 hours. The sections were pretreated with Leica Bond ER2 Buffer for 20 minutes at 95°C and Protease III (ACD, catalog no. 322102) for 20 minutes at 40°C. After staining, the sections were counterstained with hematoxylin and 10 μg/mL DAPI for 10 minutes and mounted with Mowiol mounting media.

Imaging

Images of fluorescent and IHC-stained sections were acquired on a Zeiss Axioscope Imager (chromogenic stains), Nikon Eclipse Ti microscope (IF stains), or Zeiss LSM 880 Laser Scanning Confocal Microscope (organoid stains). Raw .tif files were processed using FIJI (Image J) and/or Photoshop CS (Adobe Systems Inc.) to create stacks, adjust levels, and/or apply false coloring.

Tumor Quantification

Tumor area in H&E-stained slides were quantified using FIJI (Image J). Scanned slides were converted to 8-bit images, one intestinal roll was selected (four rolls per mouse), and an Over/Under threshold was set to capture only cells. The total intestinal area was measured using the "Measure" feature, and tumors were then identified, manually traced, and measured. All of the tumor areas were summed, then the ratio of total tumor area:total intestinal area was calculated to determine the tumor area for each mouse. Immunofluorescent images of BrdU/DAPI–positive tumors were analyzed using FIJI. Images from each channel were exported as separate .tif files, then converted to 16-bit images. The tumor area was traced manually, and the nontumor regions of the image were cleared. A threshold was set to capture only BrdU/DAPI–positive cells, then these cells were quantified using the "Analyze Particles" feature. The ratio of BrdU/DAPI–positive cells was then calculated to determine the fraction of BrdU-positive cells within a tumor. IHC images of alkaline phosphatase–positive tumors were also analyzed using FIJI. Images were converted to 16 bit, and the entire tumor area was traced manually and nontumor regions were cleared from the image. A threshold was then set for the stained areas of the tumor, and the area was quantified using the "Measure" feature. The total area of the tumor was also measured, and then ratio of alkaline phosphatase area:total tumor area was calculated to determine the fraction of alkaline phosphatase staining.

Protein Analysis

Small-intestine organoids were grown in 300 μL of Matrigel in one well of a 6-well dish for 3 days post-passage. Organoids were then recovered from the Matrigel using Cell Recovery Solution. Organoid pellets were lysed in 30 μL RIPA buffer. Antibodies used for Western blot analysis were: anti-APC (Millipore, #5535), anti-AXIN1 (Cell Signaling Technology, #2087), anti-nonphosphorylated β-catenin (Cell Signaling Technology), anti–phospho-β-catenin S33/S37/T41 (Cell Signaling Technology, #9561), total β-catenin (Cell Signaling Technology, #8480), anti-GSK3 (Cell Signaling Technology, #9832), anti–actin-HRP (Abcam, #ab49900), anti-TNKS1/2 (Santa Cruz Biotechnology, #sc-365897), anti-GFP (Abcam, #ab13970), anti-α-Tubulin (Millipore Sigma, #CP06).

Immunoprecipitation

To generate 2-D cultures, organoids were broken up by pipetting vigorously 50 times, then diluted in 5 mL of basal media. Cells were pelleted at 1,100 rpm × 4 minutes at 4°C, then resuspended in 50 μL TrypLE and incubated at 37°C for 5 minutes. PBS (5 mL) was then added to inactivate the TrypLE, and cells were pelleted. Organoids were resuspended in 2 mL basal media and plated into one well of a 6-well plate, coated with Rat Tail Collagen I (Thermo Fisher Scientific, #A10483-01) at 3 μg/mL in PBS for 30 minutes at 37°C. When confluent (after approximately 5 days), 2-D cell lines were passaged with 500 μL trypsin, neutralized in 1 mL DMEM + 10% FBS, and pelleted. Cells were then resuspended in 2 mL basal media and plated on collagen-coated plates as required. For immunoprecipitation, cells were then expanded into 2 × 15 cm plates, and when near-confluent, cultured in DMSO or G007-LK (1 μmol/L) for 24 hours. Cells were washed once with PBS, then scraped into 1 mL IP lysis buffer (10 mmol/L Tris 7.4, 150 mmol/L NaCl, 0.5 mmol/L EDTA, 0.5% NP40 + PPI/PI) and centrifuged at 13,000 rpm × 10 minutes at 4°C. Two hundred microliters of lysate was used for the immunoprecipitation using 25 μl Protein A Dynabeads (Thermo Fisher Scientific, #10001D) and incubated with AXIN1 (1 μg, Cell Signaling Technology, #2087) or IgG (1 μg, Cell Signaling Technology, #2729). Beads were washed (200 μL) and eluted (20 μL) in IP lysis buffer. Five microliters of 5× sample loading buffer was added to the elution and samples were denatured at 95°C for 5 minutes.

RNA Isolation, cDNA Synthesis, and qPCR

RNA was extracted using TRIzol (Thermo Fisher Scientific, #15596018) according to the manufacturer's instructions, and contaminating DNA was removed by DNase treatment for 10 minutes and column purification (Qiagen RNeasy #74106). cDNA was prepared from 1 μg total RNA using the qScript reverse transcription kit (Quantabio, #95047). Quantitative PCR detection was performed using SYBR Green reagents (VWR, #101414-288) and specific primers listed in Supplementary Table S4.

RNA Sequencing

Total RNA was isolated using TRIzol, DNAse treated, and purified using the RNeasy Mini Kit (Qiagen). Following RNA isolation, total RNA integrity was checked using a 2100 Bioanalyzer (Agilent Technologies). RNA concentrations were measured using a NanoDrop system (Thermo Fisher Scientific, Inc.). Preparation of RNA sample library and RNA-seq were performed by the Genomics Core Laboratory at Weill Cornell Medicine. Messenger RNA was prepared using TruSeq Stranded mRNA Sample Library Preparation kit (Illumina), according to the manufacturer's instructions. The normalized cDNA libraries were pooled and sequenced on Illumina NextSeq 500 sequencer with single-end 75 cycles.

RNA-seq Analysis

The quality of raw FASTQ files was checked with FastQC and mapped to mouse reference GRCm38 using STAR two-pass alignment (v2.4.1d; default parameters; ref. 51), and transcript abundance estimates were performed using Kallisto (52), aligned to the same (GRCm38) reference genome. Kallisto transcript count data for each sample was concatenated, and transcript per million data was reported for each gene after mapping gene symbols to ensemble IDs using the following R packages ("tximport", tximportData", "ensembldb", and "EnsDb.Mmusculus.v79"). Differential gene expression was estimated using DESeq2 (53). For data visualization and gene ranking, log fold changes were adjusted using the *lfcShrink* command in DESeq2, to minimize the effect size of poorly expressed genes. GSEA (v3.0) was performed on preranked gene sets from differential expression between DMSO and G007-LK–treated groups. We used R (v3.5.1) and R Studio (v1.1.383) to create all visualizations and perform hierarchical clustering and principal component analysis. Volcano plots, heat maps, and other visualizations were produced using the following software packages:

Enhanced Volcano (https://bioconductor.org/packages/devel/bioc/html/EnhancedVolcano.html)

Pheatmap (https://cran.r-project.org/web/packages/pheatmap/index.html)
ggplot2 (https://cran.r-project.org/web/packages/ggplot2/index.html)
ggsashimi (https://hub.docker.com/r/guigolab/ggsashimi; ref. 54)

Zygote Injections

mRNA was synthesized with mMESSAGE mMACHINE T7 ULTRA Transcription Kit (Thermo Fisher Scientific, #AM1345). Ten micrograms of DNA from the CMV-FNLS(RA) vector (Addgene, Plasmid #112671) was linearized with *Sal*I, then DNA was ethanol precipitated and used for the *in vitro* transcription reaction. For transgenesis, FNLS mRNA (100 ng or 20 ng) and 2′-*O*-methyl-3′-phosphorothioate–stabilized sgRNA (GTTCAGAGTGAGCCATG TAG; 100 ng/μL; Synthego Corp) were codelivered by microinjection. Microinjections were performed by the Memorial Sloan Kettering Cancer Center (MSKCC; New York, NY) mouse transgenic core facility, using C57BL/6J fertilized zygotes. Viable pups were genotyped by PCR and direct Sanger sequencing. Animals were maintained as heterozygotes by breeding to C57BL/6N mice.

Statistical Analyses

Statistical tests for all data presented here (other than RNA-seq) were performed in GraphPad Prism. Detailed results of each test are provided in Supplementary Table S5.

Data Availability

Raw sequence data is available at the NCBI Sequence Read Archive under accession number PRJNA524289.

Disclosure of Potential Conflicts of Interest

L.E. Dow has ownership interest (including stock, patents, etc.) in Mirimus Inc. and is a consultant/advisory board member for the same. No potential conflicts of interest were disclosed by the other authors.

Authors' Contributions

Conception and design: E.M. Schatoff, L.E. Dow
Development of methodology: E.M. Schatoff, M.P. Zafra, L.E. Dow
Acquisition of data (provided animals, acquired and managed patients, provided facilities, etc.): E.M. Schatoff, M.P. Zafra, M. Foronda, M. Shusterman, B.I. Leach, S. Goswami, B.J. Diaz, A. Katti
Analysis and interpretation of data (e.g., statistical analysis, biostatistics, computational analysis): E.M. Schatoff, M. Foronda, M. Shusterman, B.I. Leach, S. Goswami, M.P. Zafra, B.J. Diaz, A. Katti, L.E. Dow
Writing, review, and/or revision of the manuscript: E.M. Schatoff, L.E. Dow
Administrative, technical, or material support (i.e., reporting or organizing data, constructing databases): E.M. Schatoff, S. Goswami, L.E. Dow
Study supervision: L.E. Dow

Acknowledgments

This work was supported by a project grant from the NIH/NCI (CA195787-01) and a Stand Up To Cancer Colorectal Cancer Dream Team Translational Research Grant (SU2C-AACR-DT22-17). Stand Up To Cancer (SU2C) is a division of the Entertainment Industry Foundation. Research grants are administered by the American Association for Cancer Research, the scientific partner of SU2C. We thank Kevin Blighe for assistance with the Enhanced Volcano R package. We thank Shiaoching Gong and the MSKCC Mouse Transgenic Core Facility who performed zygote microinjections, supported in part by a U54 grant from the NIH/NCI (U54OD020355). We thank Katia Manova and Mesruh Turkekul from the Molecular Cytology Core Facility who performed ISH experiments, supported in part by a core grant from the NIH (P30 CA0088748). E.M. Schatoff was supported by a Medical Scientist Training Program grant from the National Institute of General Medical Sciences of the NIH under award number T32GM07739 to the Weill Cornell/Rockefeller/Sloan Kettering Tri-Institutional MD-PhD Program, and an F31 Award from the NCI/NIH under grant number 1 F31 CA224800-01. M.P. Zafra is supported in part by NCI grant NIH T32 CA203702. L.E. Dow was supported by a K22 Career Development Award from the NCI/NIH (CA 181280-01). The content is solely the responsibility of the authors and does not necessarily represent the official views of the NIH.

The costs of publication of this article were defrayed in part by the payment of page charges. This article must therefore be hereby marked *advertisement* in accordance with 18 U.S.C. Section 1734 solely to indicate this fact.

Received March 8, 2019; revised July 10, 2019; accepted July 18, 2019; published first July 23, 2019.

REFERENCES

1. Cancer Genome Atlas Network. Comprehensive molecular characterization of human colon and rectal cancer. Nature 2012;487:330–7.
2. Zehir A, Benayed R, Shah RH, Syed A, Middha S, Kim HR, et al. Mutational landscape of metastatic cancer revealed from prospective clinical sequencing of 10,000 patients. Nat Med 2017;23:703–13.
3. Stamos JL, Weis WI. The beta-catenin destruction complex. Cold Spring Harb Perspect Biol 2013;5:a007898.
4. Dow LE, O'Rourke KP, Simon J, Tschaharganeh DF, van Es JH, Clevers H, et al. Apc restoration promotes cellular differentiation and reestablishes crypt homeostasis in colorectal cancer. Cell 2015;161:1539–52.
5. O'Rourke KP, Loizou E, Livshits G, Schatoff EM, Baslan T, Manchado E, et al. Transplantation of engineered organoids enables rapid generation of metastatic mouse models of colorectal cancer. Nat Biotechnol 2017;35:577–82.
6. Huang SM, Mishina YM, Liu S, Cheung A, Stegmeier F, Michaud GA, et al. Tankyrase inhibition stabilizes axin and antagonizes Wnt signalling. Nature 2009;461:614–20.
7. Riffell JL, Lord CJ, Ashworth A. Tankyrase-targeted therapeutics: expanding opportunities in the PARP family. Nat Rev 2012;11:923–36.
8. Lehtio L, Chi NW, Krauss S. Tankyrases as drug targets. FEBS J 2013;280:3576–93.
9. Haikarainen T, Krauss S, Lehtio L. Tankyrases: structure, function and therapeutic implications in cancer. Curr Pharm Des 2014;20:6472–88.
10. Chen B, Dodge ME, Tang W, Lu J, Ma Z, Fan CW, et al. Small molecule-mediated disruption of Wnt-dependent signaling in tissue regeneration and cancer. Nat Chem Biol 2009;5:100–7.
11. Bao R, Christova T, Song S, Angers S, Yan X, Attisano L. Inhibition of tankyrases induces Axin stabilization and blocks Wnt signalling in breast cancer cells. PLoS ONE 2012;7:e48670.
12. Schoumacher M, Hurov KE, Lehar J, Yan-Neale Y, Mishina Y, Sonkin D, et al. Inhibiting Tankyrases sensitizes KRAS-mutant cancer cells to MEK inhibitors via FGFR2 feedback signaling. Cancer Res 2014;74:3294–305.
13. Norum JH, Skarpen E, Brech A, Kuiper R, Waaler J, Krauss S, et al. The tankyrase inhibitor G007-LK inhibits small intestine LGR5(+) stem cell proliferation without altering tissue morphology. Biol Res 2018;51:3.
14. Ye P, Chiang YJ, Qi Z, Li Y, Wang S, Liu Y, et al. Tankyrases maintain homeostasis of intestinal epithelium by preventing cell death. PLoS Genet 2018;14:e1007697.
15. Zhong Y, Katavolos P, Nguyen T, Lau T, Boggs J, Sambrone A, et al. Tankyrase inhibition causes reversible intestinal toxicity in mice with a therapeutic index < 1. Toxicol Pathol 2016;44:267–78.

16. Lau T, Chan E, Callow M, Waaler J, Boggs J, Blake RA, et al. A novel tankyrase small-molecule inhibitor suppresses APC mutation-driven colorectal tumor growth. Cancer Res 2013;73:3132–44.
17. Waaler J, Machon O, Tumova L, Dinh H, Korinek V, Wilson SR, et al. A novel tankyrase inhibitor decreases canonical Wnt signaling in colon carcinoma cells and reduces tumor growth in conditional APC mutant mice. Cancer Res 2012;72:2822–32.
18. Levy DB, Smith KJ, Beazer-Barclay Y, Hamilton SR, Vogelstein B, Kinzler KW. Inactivation of both APC alleles in human and mouse tumors. Cancer Res 1994;54:5953–8.
19. Tanaka N, Mashima T, Mizutani A, Sato A, Aoyama A, Gong B, et al. APC mutations as a potential biomarker for sensitivity to tankyrase inhibitors in colorectal cancer. Mol Cancer Ther 2017;16:752–62.
20. Arques O, Chicote I, Puig I, Tenbaum SP, Argiles G, Dienstmann R, et al. Tankyrase Inhibition Blocks Wnt/beta-Catenin Pathway and Reverts Resistance to PI3K and AKT inhibitors in the treatment of colorectal cancer. Clin Cancer Res 2016;22:644–56.
21. Christie M, Jorissen RN, Mouradov D, Sakthianandeswaren A, Li S, Day F, et al. Different APC genotypes in proximal and distal sporadic colorectal cancers suggest distinct WNT/beta-catenin signalling thresholds for tumourigenesis. Oncogene 2013;32:4675–82.
22. Zafra MP, Schatoff EM, Katti A, Foronda M, Breinig M, Schweitzer AY, et al. Optimized base editors enable efficient editing in cells, organoids and mice. Nat Biotechnol 2018;36:888–93.
23. Kohler EM, Chandra SH, Behrens J, Schneikert J. Beta-catenin degradation mediated by the CID domain of APC provides a model for the selection of APC mutations in colorectal, desmoid and duodenal tumours. Hum Mol Genet 2009;18:213–26.
24. Roberts DM, Pronobis MI, Poulton JS, Waldmann JD, Stephenson EM, Hanna S, et al. Deconstructing the β-catenin destruction complex: mechanistic roles for the tumor suppressor APC in regulating Wnt signaling. Mol Biol Cell 2011;22:1845–63.
25. Kohler EM, Derungs A, Daum G, Behrens J, Schneikert J. Functional definition of the mutation cluster region of adenomatous polyposis coli in colorectal tumours. Hum Mol Genet 2008;17:1978–87.
26. Zeineldin M, Neufeld KL. Understanding phenotypic variation in rodent models with germline Apc mutations. Cancer Res 2013;73:2389–99.
27. Kuraguchi M, Wang X-P, Bronson RT, Rothenberg R, Ohene-Baah NY, Lund JJ, et al. Adenomatous polyposis coli (APC) is required for normal development of skin and thymus. PLoS Genet 2006;2:e146.
28. Kim TH, Li F, Ferreiro-Neira I, Ho LL, Luyten A, Nalapareddy K, et al. Broadly permissive intestinal chromatin underlies lateral inhibition and cell plasticity. Nature 2014;506:511–5.
29. Moor AE, Harnik Y, Ben-Moshe S, Massasa EE, Rozenberg M, Eilam R, et al. Spatial reconstruction of single enterocytes uncovers broad zonation along the intestinal villus axis. Cell 2018;175:1156–67.
30. Pauli C, Hopkins BD, Prandi D, Shaw R, Fedrizzi T, Sboner A, et al. Personalized *in vitro* and *in vivo* cancer models to guide precision medicine. Cancer Discov 2017;7:462–77.
31. Moser AR, Shoemaker AR, Connelly CS, Clipson L, Gould KA, Luongo C, et al. Homozygosity for the Min allele of Apc results in disruption of mouse development prior to gastrulation. Dev Dyn 1995;203:422–33.
32. Albuquerque C, Breukel C, van der Luijt R, Fidalgo P, Lage P, Slors FJ, et al. The 'just-right' signaling model: APC somatic mutations are selected based on a specific level of activation of the beta-catenin signaling cascade. Hum Mol Genet 2002;11:1549–60.
33. Lamlum H, Ilyas M, Rowan A, Clark S, Johnson V, Bell J, et al. The type of somatic mutation at APC in familial adenomatous polyposis is determined by the site of the germline mutation: a new facet to Knudson's 'two-hit' hypothesis. Nat Med 1999;5:1071–5.
34. Crabtree M, Sieber OM, Lipton L, Hodgson SV, Lamlum H, Thomas HJ, et al. Refining the relation between 'first hits' and 'second hits' at the APC locus: the 'loose fit' model and evidence for differences in somatic mutation spectra among patients. Oncogene 2003;22:4257–65.
35. Guimaraes PPG, Tan M, Tammela T, Wu K, Chung A, Oberli M, et al. Potent in vivo lung cancer Wnt signaling inhibition via cyclodextrin-LGK974 inclusion complexes. J Control Rel 2018;290:75–87.
36. Menon M, Elliott R, Bowers L, Balan N, Rafiq R, Costa-Cabral S, et al. A novel tankyrase inhibitor, MSC2504877, enhances the effects of clinical CDK4/6 inhibitors. Sci Rep 2019;9:201.
37. Wang H, Lu B, Castillo J, Zhang Y, Yang Z, McAllister G, et al. Tankyrase inhibitor sensitizes lung cancer cells to endothelial growth factor receptor (EGFR) inhibition via stabilizing angiomotins and inhibiting YAP signaling. J Biol Chem 2016;291:15256–66.
38. Wu X, Luo F, Li J, Zhong X, Liu K. Tankyrase 1 inhibitior XAV939 increases chemosensitivity in colon cancer cell lines via inhibition of the Wnt signaling pathway. Int J Oncol 2016;48:1333–40.
39. Solberg NT, Waaler J, Lund K, Mygland L, Olsen PA, Krauss S. TANKYRASE inhibition enhances the antiproliferative effect of PI3K and EGFR Inhibition, Mutually Affecting beta-CATENIN and AKT signaling in colorectal cancer. Mol Cancer Res 2018;16:543–53.
40. Nieuwenhuis MH, Vasen HF. Correlations between mutation site in APC and phenotype of familial adenomatous polyposis (FAP): a review of the literature. Crit Rev Oncol Hematol 2007;61:153–61.
41. Nusse R, Clevers H. Wnt/beta-catenin signaling, disease, and emerging therapeutic modalities. Cell 2017;169:985–99.
42. Kahn M. Can we safely target the WNT pathway? Nat Rev 2014;13:513–32.
43. Luke JJ, Bao R, Sweis RF, Spranger S, Gajewski TF. WNT/beta-catenin pathway activation correlates with immune exclusion across human cancers. Clin Cancer Res 2019;25:3074–83.
44. Grasso CS, Giannakis M, Wells DK, Hamada T, Mu XJ, Quist M, et al. Genetic mechanisms of immune evasion in colorectal cancer. Cancer Discov 2018;8:730–49.
45. Spranger S, Bao R, Gajewski TF. Melanoma-intrinsic beta-catenin signalling prevents anti-tumour immunity. Nature 2015;523:231–5.
46. Dow LE, Premsrirut PK, Zuber J, Fellmann C, McJunkin K, Miething C, et al. A pipeline for the generation of shRNA transgenic mice. Nat Protoc 2012;7:374–93.
47. Schatoff EM, Paz Zafra M, Dow LE. Base editing the mammalian genome. Methods 2019;164–165:100–8.
48. Fellmann C, Zuber J, McJunkin K, Chang K, Malone CD, Dickins RA, et al. Functional identification of optimized RNAi triggers using a massively parallel sensor assay. Mol Cell 2011;41:733–46.
49. O'Rourke KP, Ackerman S, Dow LE, Lowe SW. Isolation, culture, and maintenance of mouse intestinal stem cells. Bio Protoc 2016;6:pii:e1733.
50. O'Rourke KP, Dow LE, Lowe SW. Immunofluorescent staining of mouse intestinal stem cells. Bio Protoc 2016;6:pii:e1732.
51. Dobin A, Davis CA, Schlesinger F, Drenkow J, Zaleski C, Jha S, et al. STAR: ultrafast universal RNA-seq aligner. Bioinformatics 2013;29:15–21.
52. Bray NL, Pimentel H, Melsted P, Pachter L. Near-optimal probabilistic RNA-seq quantification. Nat Biotechnol 2016;34:525–7.
53. Love MI, Huber W, Anders S. Moderated estimation of fold change and dispersion for RNA-seq data with DESeq2. Genome Biol 2014;15:550.
54. Garrido-Martin D, Palumbo E, Guigo R, Breschi A. ggsashimi: Sashimi plot revised for browser- and annotation-independent splicing visualization. PLoS Comput Biol 2018;14:e1006360.